Received: 30 October 2019 | Revised: 20 January 2020 | Accepted: 12 March 2020

DOI: 10.1111/str.12348

SPECIAL ISSUE ARTICLE

WILEY strain

Low-cost digital image correlation and strain measurement for geotechnical applications

G. N. Eichhorn[1] | A. Bowman[2] | S. K. Haigh[1] | S. Stanier[1]

[1]The Schofield Centre, University of Cambridge, Cambridge, UK

[2]Center for Infrastructure, Energy, and Space Testing, University of Colorado Boulder, Boulder, Colorado, USA

Correspondence
Geoff N. Eichhorn, The Schofield Centre, University of Cambridge, High Cross, Madingley Road, Cambridge CB3 0EL, UK.
Email: ge267@cam.ac.uk

Abstract

Particle image velocimetry (PIV), or digital image correlation (DIC), is a widely used technique to measure soil displacements and strains in small-scale geotechnical models. Arrays of single-board computers (SBCs) produced by Raspberry Pi, and their associated 8-MP cameras, are being used at the University of Cambridge to capture the images required for DIC analysis. This alternative to more expensive camera set-ups has numerous advantages. A single expensive and large camera can be replaced—at low cost—by multiple cameras, adding flexibility and affordability to any experimental set-up. Traditionally, the alignment of multiple cameras to each other and the referencing to a known coordinate system required painted or machined markers to be located on the observation windows through which the experiments are viewed. This can obstruct localised soil grain displacement measurements in those areas of the model where such markers are placed. To complement the Raspberry Pi camera system, a markerless calibration method was used during image acquisition. This paper outlines the set-up of four of these small computers and associated cameras, provides an overview of the use of the markerless referencing system and reviews two different experimental apparatus used to measure soil displacement and strain. When the cost of additional cabling, connectors and mounting hardware is considered for this system, the total cost to implement was approximately $125 USD per camera plus one-time costs of $175 USD for system peripherals, which represents outstanding value and enables practically all geotechnical laboratories to develop similar capabilities.

KEYWORDS

binary fiducial marker, ChArUco, digital image correlation (DIC), Raspberry PI, single-board computer (SBC), soil displacement, soil strain

1 | INTRODUCTION AND BACKGROUND

Particle image velocimetry (PIV), or digital image correlation (DIC), is a popular tool for displacement measurement and strain visualisation in geotechnical engineering research. This method replaced the older practice of installing and

Abbreviations: APT, Accelerated Pavement Tester; CMOS, complementary metal-oxide semiconductor; DIC, digital image correlation; FOV, field of view; fps, frames per second; PIV, particle image velocimetry; SBCs, single-board computers

tracking reference markers within the soil body in the late 1990s.[1] Viggiani and Hall[2] report 350 studies that have used PIV/DIC techniques in the field. Digital images of an exposed plane of the soil are taken through a transparent window on the side of the container in which the experimental event, such as an earthquake or a slope failure, is being modelled. These containers are typically several hundred millimetres to several metres in size, depending on whether the container is destined for testing in a geotechnical centrifuge[3] or on the laboratory floor. Using computer software, each image is discretised into subsets, which can overlap if desired, and the movement of each patch from one image to the next is then tracked using correlation techniques that harness the image texture provided by the contrasting colour of different grains in the soil (for sand with grains of varying colour), or seeding particles (for uniformly coloured sand and clay). The images then have to be aligned with respect to each other and a common reference coordinate system, accounting for the intrinsic lens distortion and extrinsic positioning of the cameras. Traditionally, this has been achieved using static markers that are painted onto, or machined into, the observation window. After image processing, it is possible to measure the incremental in-plane displacements of the discretised planar soil surface between successive digital images. The displacement fields can then be differentiated to determine shear and volumetric strains. A description of this technique and evidence of its versatility can be seen in numerous publications.[1,4–7] Some of the advantages of DIC in geotechnical engineering research include

- full-field measurement as opposed to localised measurement using individual transducers,[2]
- improved accuracy and precision compared to manual displacement measurements[5] and
- the ability to observe soil movement and rotation at the macroscale and microscale.[8]

Since the wide-scale adoption of DIC into geotechnical engineering research practice, improvements in accuracy can largely be attributed to improved camera technology, more robust subpixel interpolation techniques in PIV/DIC software and the development of best practices in experimental modelling that focused on optimising the contrast of the soil in images.[7,9,10] Early work with DIC in geotechnical engineering successfully utilised cameras with an image resolution of only 2 MP.[11] Cameras recently cited as being used in geotechnical work can be seen in Table 1. The costs listed do not account for accessories such as memory cards, power/data transfer cables, mounting hardware and triggering mechanisms, either physical or electrical, which may also be necessary depending on the application.

1.1 | Experimental considerations

Despite the wide variety of published DIC applications, equipment and set-ups, there are still some practical considerations such as camera size and cost that limit the use of this technique. When selecting a system of photographing geotechnical experiments, parameters considered important to successful results include[11]

- speed of experiment/frame rate,
- data storage limits and/or data transfer rates,
- automatic or manual focusing/brightness adjustments,
- remote shutter triggering mechanism and
- marker placement and translation to an x–y coordinate system.

Owing to the size limitations of many physical modelling experimental set-ups, particularly those destined for testing in a geotechnical centrifuge,[3] it is necessary to optimise camera placement, which can be challenging due to space

TABLE 1 Examples of camera models used in recent geotechnical DIC publications

Camera model	Image resolution (MP)	Maximum image capture rate (Hz)	Camera size	Camera cost, USD (+ lens)[a]	Reference
Prosilica GC2450C	5	15	46 × 33 × 105 mm	$2,760 ($300)	Stanier and White[9]
Canon S40/50	3.8/5	0.5	112 × 58 × 62 mm	$800	Stanier and White[9]
Canon G10	14.7	1	109 × 78 × 46 mm	$500	Bowman and Haigh[12]
GoPro HERO3	12	2	42 × 60 × 20 mm	$450	Tan et al.[13]
Canon EOS 450D	12	4	129 × 98 × 62 mm	$670 ($200)	Peerun[14]
Phantom v5.1	1	1,200	12.5 × 11 × 25 cm	$25,000	Kokkali et al.[15]
MotionBLITZ EoSens mini2	3	523	65 × 65 × 65 mm	$20,000	Heron et al.[16]

[a] At time of manufacture.

restrictions if the cameras themselves are large. Until recently, consumer-grade cameras have been used for experimental geotechnical engineering research. The size of these cameras is typically more than 50 to 100 mm in the longest dimension of the camera body. This places some restrictions on where the camera can be placed in an experimental set-up. The distance from the camera lens to the plane of the model being imaged must be greater than the minimum focus distance. This is typically not less than 200 to 300 mm for consumer-grade cameras, placing a limit on the space required between the camera and observation window of the experiment.

Further, tracking small displacements and strains occurring within the soil can be difficult due to the lens-induced distortions, which must be corrected for using photogrammetric techniques.[5] At the other end of the spectrum, tracking large displacement and strains is also challenging, because analysis subsets often leave the field of view (FOV) of the camera if only a subset of the exposed face of the model is being imaged by a particular camera. In this instances, it is common to use multiple cameras in an experimental set-up to cover a larger FOV. A somewhat subjective centroiding algorithm is used to determine coincident image space (in pixels) and object space (in millimetres, or other real-world units) locations of the painted or machined markers, which allows standard photogrammetric techniques (pin hole camera and lens distortion models) to be used to remove distortion and align the images. However, this leaves some areas of the observation window—and the exposed plane of the model—occluded by the markers.

The following sections detail a new method for photographing soil in geotechnical experiments using single-board computers (SBCs) and very small image sensors typically used in modern mobile phones. A method for markerless alignment was developed to support the use of these cameras, although traditional control markers could also be used with the SBC set-up that we present. An example of each method is presented in Section 4.1.

2 | MARKERLESS CAMERA ALIGNMENT

One of the advantages of DIC techniques is that the need for target markers within the soil is removed, and instead, the measurement relies on the image texture either naturally provided by the contrasting colour of the soil grains or artificially provided through the addition of highly contrasting seeding particles (typically dyed sand or brightly coloured plastic flock[9]), to track movement from one image to the next.[5,11] Image analysis techniques convert pixel displacement, or u–v space, to a physical measurement in the plane of the observation window known as x–y space. This is achieved using stationary control markers, or reference markers, affixed to the window.[5] These markers are typically round, black and white and obscure a portion of the FOV. The location of these control markers is measured before the experiment begins or is known if they are accurately machined into the surface of a window. During post-processing of the data, the soil displacements and strains can be referenced back to this user-defined real-world coordinate system.

Control markers are also required to counter the distortion of optical lenses. Optical cameras introduce distortions into the photo caused by the intrinsic lens properties. A lens distortion model can be used to measure lens distortion parameters such as the radial and tangential lens distortion caused by the optics placed in front of the image sensor.[17] This is true at any scale but especially during centrifuge testing where an experiment experiences an increased gravitational field by centrifugal acceleration that can cause additional lens distortion compared to that which occurs at Earth's gravity on the laboratory floor. Finally, when multiple cameras are used, the control markers allow multiple arrays of images to be aligned and stitched together to create contiguous displacement and strain fields.[18]

The process to locate the reference markers typically uses centroiding methods. This requires manual identification of each reference point, which is both time consuming and computer processor intensive.[4] These markers will also obscure a portion of the FOV, and if the localised soil movement cannot be anticipated (common in geotechnics), an area of interest in the soil experiment may be missed if the camera is not placed correctly or if the area does not contain reference markers.

For the first time in geotechnical laboratory modelling, we have implemented an alternative referencing method that allows multicamera registration to the same x–y plane, and coalignment of displacement vector fields from multicamera systems, without the use of static markers. In computer vision applications, the term 'pose estimation' is used to refer to the orientation of a point in 3D space. Historically, a computer-generated chessboard has often been used to calculate the parameters for camera lens distortion models and to estimate camera pose. This technique arose because of the highly structured nature of a chessboard, and the development of corner extraction algorithms, which facilitated the identification of concurrent image space (in pixels) and object space locations (in millimetres, or other real-world units), from which camera pose can be estimated. A further advance on this technique was achieved through the development of binary square fiducial markers,[19] referred to commercially as an ArUco marker. A grid of ArUco markers can be generated based on dictionaries of uniquely identifiable markers and assembled into linearly spaced m by n arrays. Computer

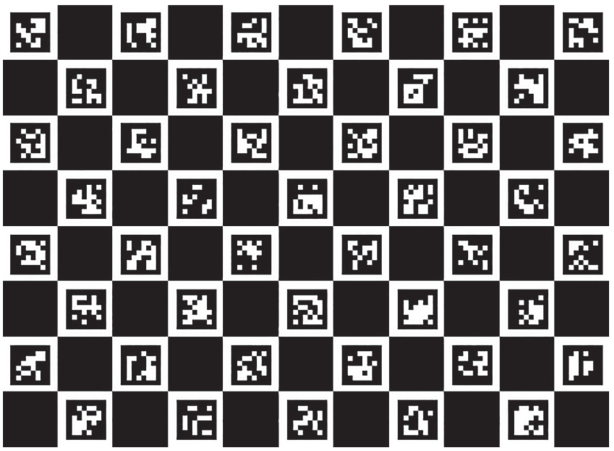

FIGURE 1 Typical ChArUco camera calibration board

software exists, which automatically identifies unique ArUco markers for each square in an m by n grid, as well as their relative spatial alignment to each other.

Recently, the two approaches described above were combined into a package called ChArUco, combining both the chessboard and the ArUco markers into one composite calibration board. This combines the automated ArUco detection with the more accurate corner extraction afforded by the chessboard because the ArUco markers are located first, from which the chessboard corner locations are approximated, before the actual chessboard coordinates are determined using conventional corner extraction algorithms. This results in fast, automated and accurate calibration of the intrinsic and extrinsic properties of the camera. These camera registration and distortion correction techniques have been incorporated into the widely used computer vision package called OpenCV (Open Source Computer Vision), developed by Intel,[20] for which both C++ and Python bindings exist. An example of a ChArUco board is shown in Figure 1.

The process described below has been used for markerless registration of PIV/DIC images from pixel space into physical model dimensions, without the need to input or manually identify the ArUco marker locations. The automated calibration and PIV/DIC data transform procedure consists of the following steps:

1 Generate a ChArUco board using OpenCV and print on paper. Affix to a rigid board.
2 Photograph the ChArUco board in different orientations relative to the cameras, at the approximate focal length that the experiment will be conducted at. Our experience found that a minimum set of 50 photographs should be used to obtain an accurate calibration.
3 Process each set of images generated in Step 2 using the camera calibration module in OpenCV, in order to calibrate the intrinsic camera matrix and lens distortion parameters. These parameters are the radial and tangential distortion parameters $[k1, k2, p1, p2, k3]$, and the camera matrix giving focal length $[fx, fy]$ and the optical centre $[cx, cy]$. This is typically referred to as a pinhole camera model.
4 Separately, and in addition to Step 2, capture single images from each camera of the ChArUco board pressed against the observation window, with the cameras in the positions they will be placed in during the experiment. These images will be used to measure the rotation matrix and transform vector to transform from pixel space (u–v) to object space (x–y).
5 Process the single images from Step 4 using the intrinsic camera distortion parameters from Step 3, the ChArUco board information from Step 1 and the ChArUco marker identifications from Step 3. This is achieved using a script developed using various OpenCV modules and functions. The output of this process is a 3×1 rotation vector and a 3×1 translation vector, representing the Euler transformations of the camera plane to the ChArUco board where the image frame was captured.
6 Convert the 3×1 rotation vector to a 3×3 rotation matrix and a 3×1 transform vector in the world coordinates of the ChArUco board using a Rodrigues transform, found in most numerical processing programs. The global origin of the ChArUco board is marker number 1, which is always found in the lower left corner of the ChArUco calibration board.
7 Process the images obtained during the geotechnical experiment using a suitable PIV/DIC algorithm. We use the MATLAB package GeoPIV-RG,[21] but the techniques described here could be used with any PIV/DIC algorithm that facilitates direct operation on the output displacement field data. The product of the PIV/DIC algorithm is a file with subset locations in pixel space.
8 The displacement matrix in pixel space must be undistorted to counter the lens tangential and radial distortion. This is achieved using the parameters obtained from Step 3. This method uses an built-in function in the OpenCV package to

accept the patch locations and the distortion parameters, and outputs undistorted patch locations in pixel space. The data must then undergo a transformation and rotation described below.

9 Transform the image subset locations calculated using the PIV/DIC algorithm in Step 7 from images space (u, v) to object space (x, y). The transform requires the 3×3 rotation matrix and transform vector from Step 6, a scaling factor to convert from image space units (pixels) to object space units (e.g. millimetres) and the coordinates of the centre of each image in pixels, which is constant. The scale factor can be determined directly from the ChArUco camera calibration board corner locations after correction for intrinsic lens distortions.

10 The output is a georectified set of PIV/DIC subsets in x–y space for each camera, all utilising the same real-world reference system, allowing data streams from different cameras to be merged into one.

Owing to this method's ability to measure the camera's focal length and optical centres, and therefore the camera lens distortion parameters, this method is ideally suited to replacing centroiding methods of photo alignment for geotechnical laboratory applications. The use of the ChArUco alignment method means both a reduction in processing time through the widely used GeoPIV-RG software package (since centroiding can be eliminated) and cost savings of custom milled transparent observation windows that no longer need markers to be permanently countersunk. This also means that the transparent observation windows can be reused for multiple experimental set-ups.

The use of this markerless method for referencing PIV/DIC measurements is only possible if the camera remains stationary relative to the observation window. This has been a particular concern of the geotechnical centrifuge modelling community since cameras experience an increase in self-weight due to the centrifugal acceleration they experience during testing. Historically, there was a concern that the relatively large and heavy camera lenses would experience a distortion of the camera body and associated optical components. In the following section, we present the application of new low-cost imaging technologies for photographing geotechnical experiments that complements this markerless alignment technique and which we demonstrate is not affected adversely by the increase in camera self-weight during centrifuge-based testing.

3 | SBC CAMERA METHODS

The geotechnical research group at the University of Cambridge is mitigating the challenges associated with the use of traditional consumer cameras for PIV/DIC through the use of cameras more typically associated with mass market 'smartphones' via SBCs. Arguably, the world's most popular SBC is the Raspberry Pi, which was developed in 2012 in Cambridge, with the goal of offering low-cost computers to school-age children and maker enthusiasts.[22] We have developed PIV/DIC experimental apparatus utilising arrays of Raspberry Pi SBCs, which due to their small form factor, results in optimised camera placement, a low cost to entry and elimininates the small space requirements needed for the system to be deployed on both the laboratory floor and the confines of centrifuge modelling packages.

3.1 | Hardware

SBCs have become increasingly affordable and are equipped with significant computing power. A typical unit includes a main 64-bit processing chip, DC input power, HDMI out, Ethernet port, USB ports and other global interfaces. The design does not include a built-in hard disk or solid-state hard drive; instead, it relies on an microSD memory card to support the Linux-derived operating system and to provide storage space. This, along with the small physical size, open-source software and community support, has now made SBCs a viable option for scientific measurement and observation.[22] One of the main advantages of this SBC is the low cost to entry, averaging $35 USD. The specifications are shown in Table 2.

The Raspberry Pi also has a peripheral camera attachment that can be paired with the computer. A selection of the Camera Model 2.1 specifications is shown in Table 3. The camera boards, weighing only 3 g and measuring 25×24 mm, are much lighter than most other computer vision cameras and significantly cheaper at a cost of approximately $25 USD at the time of writing. Each camera requires its own Raspberry Pi; however, it does not need to be located close to the computer, with HDMI cables and adapters allowing the camera to be several metres away from the Rapsberry Pi SBC. The small size of both the camera and the SBC makes it easy to assemble arrays of these camera–computer pairs at low cost compared to other computer vision cameras or more traditional consumer-grade 'point-and-shoot' digital cameras. This camera hardware is particularly advantageous when small space requirements limit the size of hardware as is demonstrated later in the first example application.

TABLE 2 Raspberry Pi 3B specifications

SBC parameter	Details
Board dimensions	85 × 49 mm
SOC	Broadcom BCM2837B0 Cortex-A53 64-bit
CPU	1.4 GHz 64-bit quad-core
RAM	1 Gb LPDDR2 SDRAM
WiFi	Dual-band 802.11ac wireless
Ethernet	10/100
Video out	HDMI
USB 2.0	4 ports
Power	5-V/2.5-A DC input
Operating system	Linux and Unix

TABLE 3 Camera model v2.1

Camera parameters	Details
Size	25 × 24 × 9 mm
Weight	3 g
Still resolution	8 MP
Video modes	1080p30, 720p60 and 640 × 480p60/90
Linux integration	V4L2 driver available
C programming API	OpenMAX IL and others available
Sensor	Sony IMX219
Sensor size	3,280 × 2,464 px
Sensor resolution	8.08 MP
Sensor image area	3.68 × 2.76 mm (4.6 mm diagonal)
Pixel size	1.12 × 1.12 μm
Focal length	3.04 mm
Minimum focus distance	5 mm
Horizontal field of view	62.2° (or 1.2 × camera distance)
Vertical field of view	48.8° (0.9 × camera distance)
Focal ratio (f-stop)	2.0

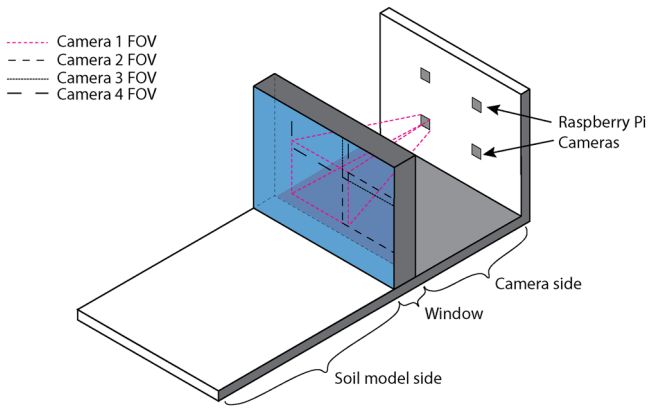

FIGURE 2 Typical PIV/DIC test set-up for geotechnical physical modelling applications using a Perspex window and multicamera cross-sectional FOV

The basic set-up for a geotechnical PIV/DIC test can be seen in Figure 2, showing an array of four cameras in a square configuration focused on a transparent window exposing a plane of the soil model. The FOV for each camera is represented by the black dashed lines on the window surface. The cameras would be arranged so that there is minimal FOV overlap at the window, which is indicated for one camera by the grey dotted lines. Owing to the new camera alignment technique described in Section 3, cameras only require negligible overlap, with only as much required as is necessary to eliminate lost areas of interest. Unlike image stitching programs that require as much as 30% image overlap to align adjacent photos, the overlap in the markerless method described here plays no part in aligning multiple cameras to each other.

The cameras can capture still photographs at a resolution of 3,280 × 2,464 px, or 1080p high-definition video at a resolution of 1,920 × 1,080 px and a frame rate of 30 frames per second (fps). Higher frame rates have been achieved with custom manipulation of the camera interface through the software library OpenCV, and capture rates as high as 120 fps have

been reported in the computer vision community.[23] The camera interface uses a rolling shutter that has been avoided in the past by the scientific community due to the piecewise, rolling collection of data, line by line from the complementary metal-oxide semiconductor (CMOS) image sensor. For highly dynamic events, and long exposure times, the rolling shutter can cause a mismatch in strain measurements from the top of an image to the bottom.[9] However, for moderately dynamic events with appropriate lighting, short exposure times and high-power SBCs such as the Raspberry Pi 3B+, this is less of a concern. The Raspberry Pi 3B+, when paired with the Camera Model 2.1, has a capture time for each row of pixels of 20 ns, making the minimum capture time for a full-frame still image approximately 49 μs.

The camera boards are traditionally connected to the Raspberry Pi computer through a 15-way flat flexible cable (FFC) to the camera serial interface (CSI) port on the Raspberry Pi. However, this was found to be susceptible to electromagnetic (EM) interferences between adjacent FFC cables. This was particularly problematic if the FFC cables were spaced closer than 2 mm apart. In the experimental set-ups presented in the following sections, the FFC cables were converted to an ultra-thin HDMI cable. A conversion board to do this is available for purchase from enthusiast maker websites such as www.tindie.com. The use of HDMI cables to transmit camera data was found to solve the EM interference problem and simplify routing of the camera connection to the Raspberry Pi SBC where a second conversion board changes the connection back to an FFC to interface with the Raspberry Pi.

The Raspberry Pis were also retrofitted to replace the microUSB 5-V power connection, which was found to be unreliable when the equipment was moved or interacted with. A permanent power lead was soldered to the 5-V terminals on the back of the SBC, and a common 5-V DC power supply is used for all of the SBCs in the experimental set-up. A full accounting of the costs and the peripherals described in this section is found in Appendix A.

3.2 | Camera triggering

One of the features of the Raspberry Pi SBC is the general-purpose input/output (GPIO) electronic interface. This is a built-in 40-way insulation displacement connector (IDC) connection that can be used to send and receive 3.3-V DC signals. This has been utilised in the camera set-up described in this paper for triggering of multiple cameras simultaneously. The IDC header pins can be used individually as needed and controlled through a Python/UNIX interface in the operating system on the Raspberry Pi computer. Camera synchronisation has been achieved by electronically triggering the cameras simultaneously through a custom junction box paired with a solid-state relay (SSR) and controlled by a single master Raspberry Pi, connected through the junction box to a number of slave Raspberry Pi SBCs. The wiring diagram for the triggering SSR is shown in Figure 3.

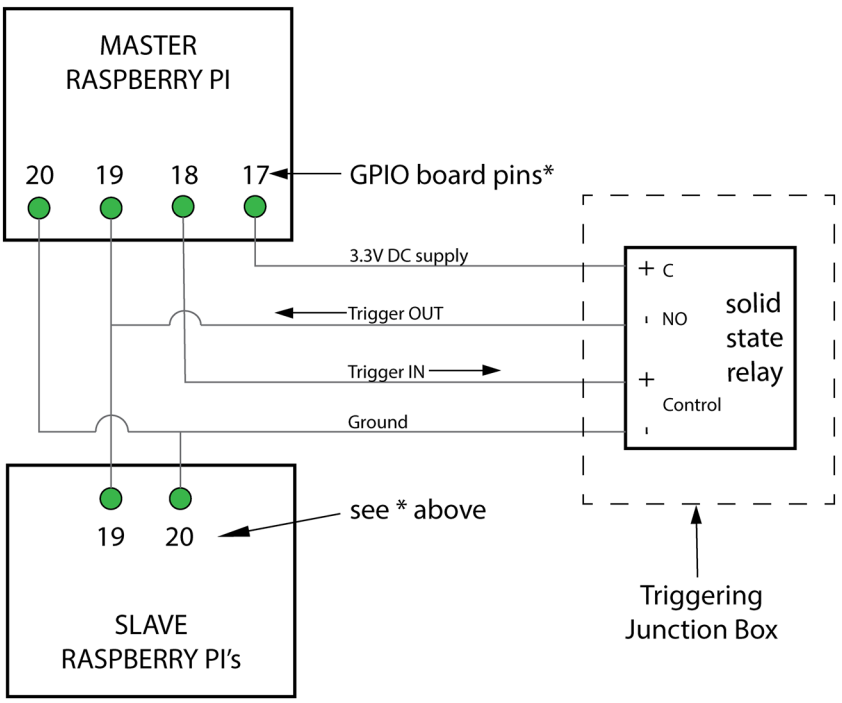

FIGURE 3 Camera triggering junction box wiring

The triggering GPIO pins used and shown in Figure 3 are customisable and not absolute but rather can be selected by the user based on needs and availability of the GPIO pins. Each of the slave Raspberry Pis is connected via a 40-way IDC header and 40-way IDC cable—wrapped with helical plastic sleeving for durability—to the triggering junction box. Triggering of 12 cameras simultaneously has been achieved to within 10 μs using this system.

3.3 | Software configuration

The cameras are supported by a programmable library in Linux that is open source and has a strong community support network, making programming of these cameras for bespoke purpose image capture accessible to many research fields. The native language that the camera module runs on is C; however, there are additional software abstraction layers that allow direct programming of the camera in Python. This feature makes the Raspberry Pi camera system ideal for doing near-real-time image analysis using numerical analysis libraries in Python such as NumPy and SciPy. There is also wide compatibility with the computer vision package OpenCV.

We present a method to interface with the Raspberry Pi camera board using a pure Python interface through the software library 'picamera'. This abstraction layer provides the user with a library of Python commands to manipulate the GPU on the Raspberry Pi and control the camera settings through software manipulation of the data captured by the CMOS image sensor. The Raspberry Pis are configured such that they have a start-up program that automatically runs on each of the slave Raspberry Pi computers (e.g. in a series of six cameras paired with six Raspberry Pis). The start-up sequence launches two systemd scripts. A systemd script is a Linux start-up command that allows programs to be run automatically when a computer is booted. The first script is a network interface, which allows image capture directly to an attached network storage location via an Ethernet connection. The second systemd script launches a Python script to capture images or video and loops in a listening routine monitoring the GPIO pins for an input signal from the master trigger SBC. By running this second script automatically during boot up, only the master SBC needs to be manipulated during an experiment since the slave SBCs are already initialised to start capturing images or video.

3.4 | System performance

The Raspberry Pi cameras have been tested in two laboratory applications and are discussed in Section 4.1. For each experimental set-up described, the geotechnical DIC software geoPIV was used. The performances of the DIC algorithms used in geoPIV and geoPIV RG have been measured experimentally.[21] The performances were obtained using synthetically generated images that encapsulated the displacement of Gaussian intensity projections to subpixel resolution. Both of the DIC algorithms presented average the colour channels to produce a greyscale image on which the DIC computations are performed. The Raspberry Pi camera makes use of a Bayer filter as part of the CMOS chip. The geoPIV algorithms average the RGB colour channels to obtain an average pixel intensity level based on the Bayer-filtered RGB data from the Raspberry Pi camera.

The strain window used in both DIC packages is triangular and uses three data points of displacement to derive strains using shape functions for a linear strain triangle. The strain resolution has been experimentally determined for both DIC packages using synthetically generated images and is presented in Tables 4 and 5. We use the same methodology that White et al.[5] used for their strain resolution calculation, yielding values of 468 and 37.5 μm/m for geoPIV and geoPIV RG, respectively. These are based on experimentally determined strain resolutions of the DIC algorithms for geoPIV, which was measured as 0.01 px (in-plane), for the noise floor.[5] Determination of the strain resolution for the DIC package geoPIV RG followed the same methodology and was measured experimentally at 0.001 px (in-plane).[21] The displacement measurement floor was determined using both DIC algorithms by generating synthetic images of a black background, onto which white Gaussian dots were projected. A uniform subpixel translation was then applied to the Gaussian dots before a second image was created. The variance between the known displacement and that measured gives the noise floor. The strain noise floor was calculated using the displacement noise floor and the subset spacing, following the best practices guide published by the International Digital Image Correlation Society.[24]

The Raspberry Pi camera grey-level noise was approximated by taking the average of the standard deviation of the average of the pixel intensity of the RGB colour channels, taken after they have been processed with a Bayer filter. Since the Raspberry Pi camera is capturing 8-bit RGB images, this averaging of the colour channels reflects the DIC processing that occurs in the geoPIV software package. The grey-level noise for the Version 2.1 Raspberry Pi camera is 0.4%. Seperately, the grey-level noise of each colour channel was calculated, and this fell within 0.02% of the mean of all three-colour channels, therefore supporting the averaging approach taken with the three separate colour channels.

TABLE 4 DIC analysis parameters for slope failure model

Analysis parameter	Details
DIC software	GeoPIV-RG Version 01/04/2019
Image filtering	None
Subset size	80 px/2.1 mm
Step size	80 px/2.1 mm
Subset shape function	First-order
Matching criterion	ZNCC
Interpolant	Biquintic B-spline
Strain window	Triangular
Virtual strain gauge size	80 px/2.1 mm
Strain formulation	Engineering strain
Postfiltering of strain	None
Displacement noise floor	1×10^{-3} px (in-plane)
Strain noise floor	37.5 μm/m

TABLE 5 DIC analysis parameters for APT tyre test

Analysis parameter	Details
DIC software	GeoPIV Version 9
Image filtering	None
Subset size	64 px/5.12 mm
Step size	64 px/5.12 mm
Subset shape function	Zeroth-order
Matching criterion	NCC
Interpolant	Bicubic
Strain window	Triangular
Virtual strain gauge size	64 px/5.12 mm
Strain formulation	Engineering strain
Postfiltering of strain	None
Displacement noise floor	1×10^{-2} px (in-plane)
Strain noise floor	468 μm/m

4 | EXAMPLE APPLICATIONS

4.1 | Geotechnical centrifuge slope failure

Computer modelling cannot reproduce complex ground deformations in cases where the underlying physics is poorly understood, but it is possible to use physical modelling to recreate Earth processes that are not well characterised. Centrifuge modelling, a type of physical modelling, utilises small models that are accelerated at many times Earth's gravity, and the principles of similitude,[25] to reproduce the mechanical and time-dependent response of the full-scale prototype problem.[3] This is important for geotechnical problems because the mechanical response of soils is stress dependent, and the enhanced acceleration provided to the small-scale models by the centrifuge preserves stress similitude. Centrifuge modelling is being carried out at the University of Cambridge using a 1-m-diameter geotechnical drum centrifuge to model slope failures in sandy soil.[26]

To showcase the systems described in this paper, a study was performed to examine the slope failure of an embankment that was loaded at the crest of the hill by a shallow strip footing. The slope failure was initiated by loading the footing until the soil sheared. The soil displacement mechanisms were recorded using 1080p HD video captured on four Raspberry Pi 3B+ SBCs and Model 2.1 cameras. The geotechnical drum centrifuge uses a curved aluminium container with a toughened glass window within the container to separate the soil side from the camera side of the experiment. This configuration is shown in Figure 4.

One of the challenges faced by geotechnical centrifuge modellers is the limited space with which to prepare and execute an experiment. The inner ring channel of the drum centrifuge has a width of 220 mm, and a maximum model depth of 150 mm, at a radius of 350 mm to the top of the model container. The soil side of the experiment is 125 mm wide, and the container is approximately 300 mm in length around the outer diameter of the container. These dimensions constrain the size of experiment that can be carried out in the centrifuge. The cameras have a distance from the side wall of the container to the glass of only 100 mm. Traditional cameras, including modern machine vision cameras, are unable to operate in this small space owing to the minimum focus distance that is typically more than 100 mm. For this reason, the

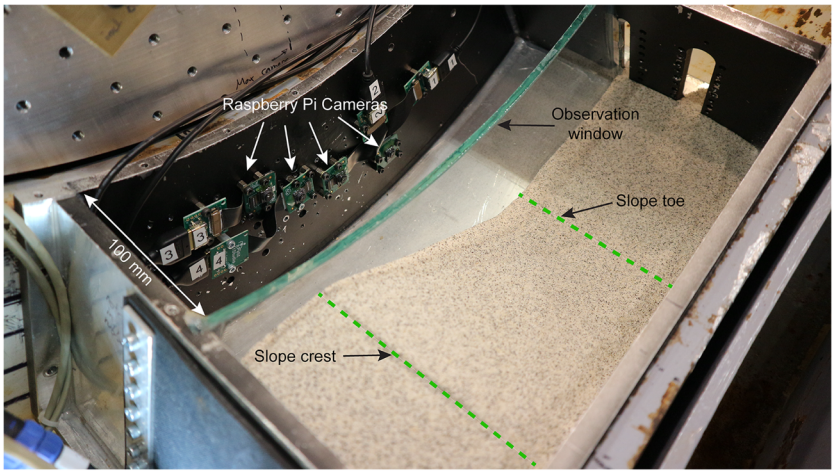

FIGURE 4 Oblique view of centrifuge model set-up showing slope and camera configuration

Raspberry Pi single-board camera, with a thickness of only 5 mm, was ideally suited for this environment. The cameras were affixed to the sidewall of the aluminium model container with four M3 bolts and hex standoffs. These were tightened such that there was no appreciable movement in the camera board when manually manipulated. This feature is critical to eliminate camera board displacement in a centrifuge. An additional modification is needed to use these cameras in high-gravity environments. The stock camera is composed of a circuit board and a separate floating image sensor that is affixed to the board with two-sided tape. This floating sensor will deflect under accelerated gravity and must be glued permanently with epoxy to the camera board. Without this modification, the use of ChArUco alignment methods will not work for centrifuge experiments.

A slope was constructed of Hostun sand with 10% of the sand dyed black using waterproof black ink to improve the image texture, or contrast, provided by the soil, an important step for maximising the accuracy and precision of the PIV/DIC measurement of soil displacement.[9] The soil was air pluviated, and the slope was constructed at an angle of 30°. The relative density of the soil was approximately 65% and has a mean particle size or D_{50} of 0.335 mm. A 100 × 40-mm aluminium footing was cut to match the width of the soil side of the experiment. This footing was placed at the top of the slope on the crest. The model was instrumented with four Raspberry Pi 3B+ SBC camera pairs and accelerated to 100 *g*. During spin-up of the centrifuge, the cameras were triggered to record video to monitor for any deflection of the camera due to centrifugal loading. In a separate experiment where the glass window was prepared with traditional PIV circular reference markers, the same spin-up procedure was followed. The reference markers were tracked using a combination of centroiding and GeoPIV-RG.[9] The displacement of the centroided reference markers was evaluated after experiment. We report that there was an average displacement of the centroided reference markers from 1- to 100-*g* acceleration, of less than 0.001 mm. More importantly, no systematic distortion of the grid of centroided reference markers was observed, indicating that the lens distortion remained the same throughout the experiment. This amount of displacement in the plane of the observation window is small enough that the use of markerless referencing methods—such as the ChAUuco binary fiducial markers—is acceptable, even in an increased gravity environment such as a geotechnical centrifuge.

Prior to the slope failure experiment, images were captured of a ChAruco camera calibration board, which was generated using a Python script and printed out and affixed to rigid board. The board was generated and printed such that each side of the checker board was 7 mm in length. This board was placed on the soil side of the experiment, and single photos were taken using each camera. These four photos were used to assess the relative position of the plane of the image of each camera in the real-world coordinate system of the ChArUco board, and by extension, the *x*–*y* space of the model container. The procedure outlined in Section 3 was followed to measure the distortion parameters for each camera. The video of the slope displacement caused by the loaded strip footing was sliced into frames and passed through the GeoPIV-RG MATLAB package, giving displacements in pixel space of each image. The DIC image processing parameters used are listed in Table 4. A transform was then applied to each set of positions of the PIV patches consisting of a rotation, constant scaling and translation. These were determined from an analysis of the four single photos captured from each camera for assessing the world coordinates of each camera relative to an origin on the plane of the ChArUco board. The soil displacement measurements from each of the four cameras were then able to be plotted in the same real-world reference frame, as shown in Figure 5. The incremental strains were calculated for each camera, and the major principal

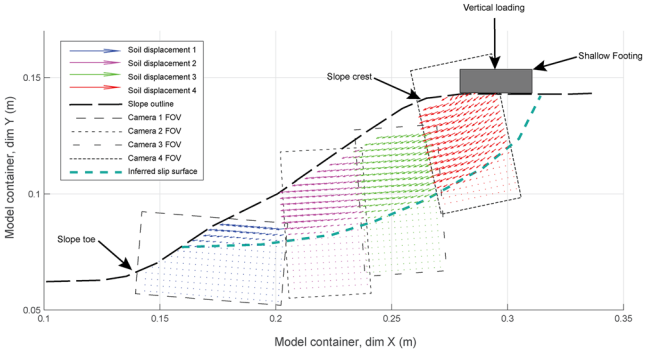

FIGURE 5 Centrifuge slope failure displacement field and experiment set-up

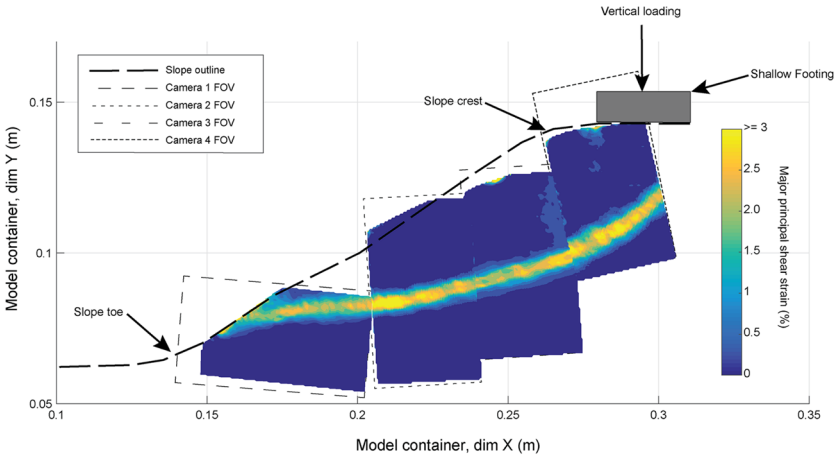

FIGURE 6 Centrifuge slope failure major principal strains

strain field is shown for the slope in Figure 6. This shows that it is possible to identify the shear band localisation at the slip surface within the slope.

These results show that measurements derived from multiple cameras can be oriented relative to each other via a global coordinate system in geotechnical experiments, without the use of in-flight reference markers painted onto, or machined into, the observation window. This is tremendously useful since it eliminates an intensive post-processing step, improves the utlisisation of the camera FOV and makes expensive machined and polished Perspex windows reusable for different applications. The Raspberry Pi computers and cameras have been tested in the geotechnical centrifuge environment and showed no sign of malfunction during repeated testing over a period of 2 years. The solid-state components and simple optics paired with an 8-MP camera and programmable library to interface with the hardware make this technology very attractive for small-scale geotechnical centrifuge modelling applications. Note that in the example here, the four camera displacement fields overlap in some areas. These vectors have been left in place to illustrate the similarity and overlap of the displacements. These fields can further be merged into one complete matrix of displacements. To do this, redundant vectors where cameras overlap will need to be resolved or an average displacement calculated. The Raspberry Pi 8-MP cameras also allow for maximisation of the D_{50}/p ratio, where D_{50} is the average soil particle size and p is the size of a pixel in object space. Previous PIV/DIC optimisation work in geotechnics has identified that a minimum D_{50}/p ratio of between 4 and 8 should be targeted for good-quality PIV/DIC soil displacement measurements.[10] The proximity of the Raspberry Pi cameras to the soil plane in this experiment resulted in a D_{50}/p ratio in excess of 10.

4.2 | Accelerated pavement testing

As an example of how the Raspberry Pi SBC and associated cameras are used in a 1-*g*, large-scale application, a similar system was set-up to support the Cambridge Accelerated Pavement Tester (APT). The APT was built in 2015 in order to understand granular movements beneath a flexible pavement. The research relies heavily on the use of PIV/DIC.[12] A flexible pavement structure was constructed in a concrete pit with dimensions of 1,000 × 800 × 860 mm. In the initial experiments, images were captured perpendicular to the movement of the tyre using two Canon G10 cameras (Table 1). It was found that a rut on the surface was partially created due to the upheaval occurring symmetrically on both sides of the wheel. A sliding block mechanism can be used to characterise this deformation behaviour. However,

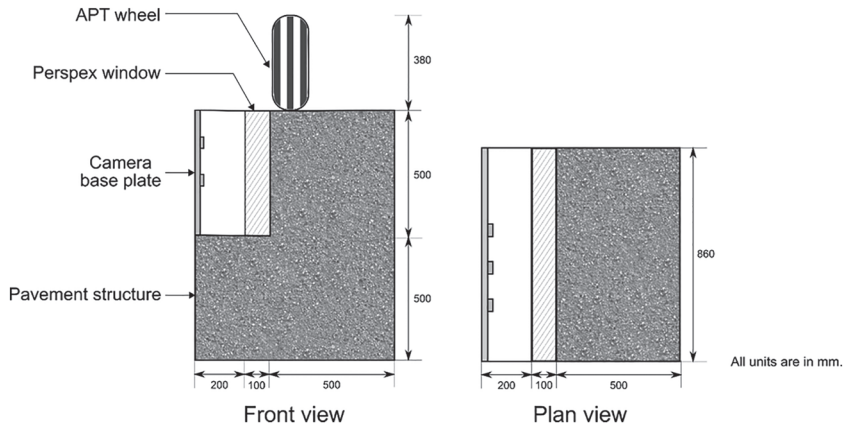

FIGURE 7 Schematic of the APT

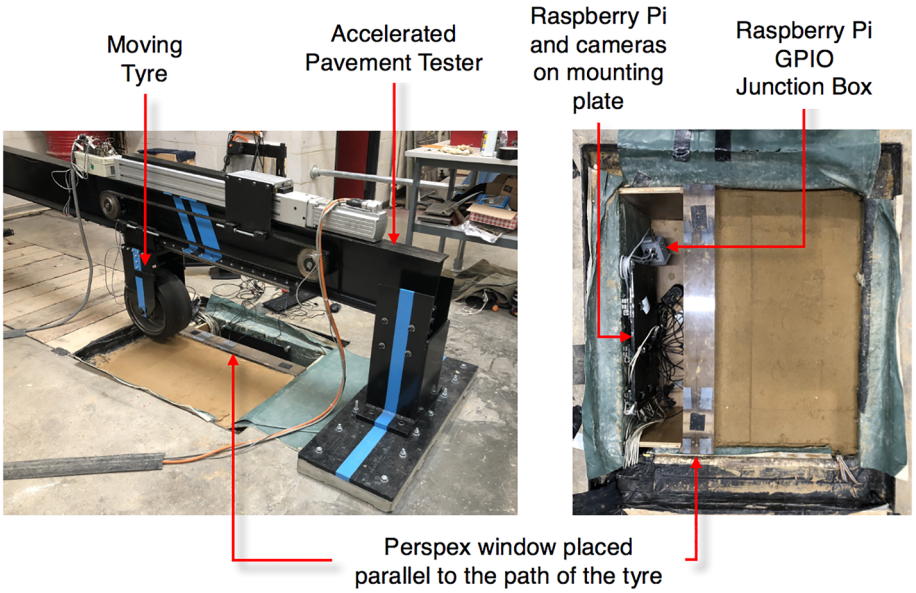

FIGURE 8 Side and plan view photos of the APT with the Raspberry Pi imaging set-up

the deformation field is three-dimensional, and further research was necessary to examine the asymmetrical flow zones in front of and behind the moving tyre in order to comprehensively understand the rutting mechanism. Limitations on the space available for cameras and support equipment made this an ideal application for the Raspberry Pi SBCs and cameras.

The set-up of the experiment can be seen in Figures 7 and 8. A 1,000 × 500 × 100-mm-thick Perspex window was fitted into place in the concrete tank parallel to the movement of the tyre. Only 200 mm separated the front of the Perspex window and the wall of the tank. Control points were added to the window to help with image-object space calibration, or centroiding, during post-processing of the data. A single Raspberry Pi SBC 'master' and six Raspberry-Pi 'slaves' and associated cameras were mounted to a steel base plate, coated with antireflective matt black paint and fixed on the side of the pit to capture the soil profile through the window. These six cameras, placed in two rows and three columns, were required to capture the full FOV. The cameras were triggered via the APT's main data acquisition computer through a remote connection to the master Raspberry Pi. A Python execution function operating on the master Raspberry Pi provided the triggering signal to the GPIO junction box, which triggered the slave SBCs and cameras ensuring that images were captured simultaneously.

The project focused on tracking soil movement under the wheel axis as it travelled at a steady rate. The cameras triggered at 1 fps. As the wheel moves within a stationary frame of reference, traditional PIV/DIC is problematic. If a rapid frame rate is used, little movement is seen between images, while for a slow-frame rate, the wheel position changes substantially leading to a smeared strain field. To resolve the paradox, an alternative coordinate system based on the current wheel position was used and each incremental displacement field was mapped into this space (Figure 9). The DIC image processing parameters used are listed in Table 5. Averaging between overlapping frames then allowed a high-precision displacement field to be calculated with a FOV much wider than that of an individual image.

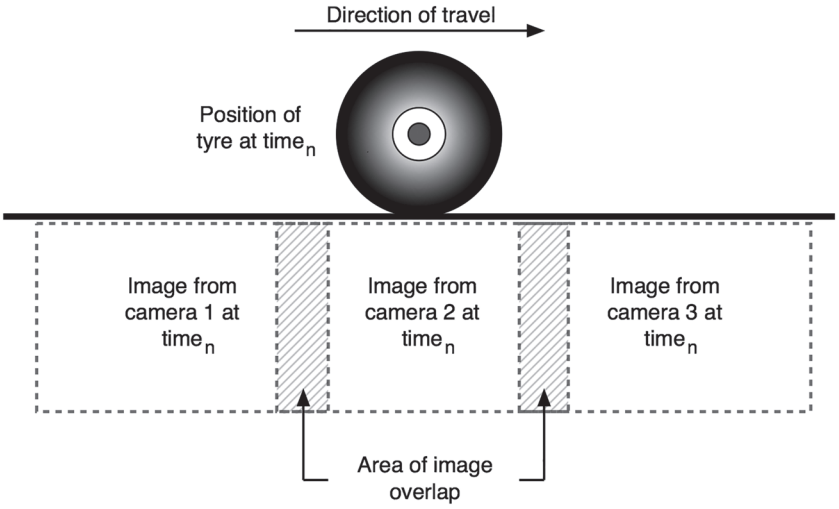

FIGURE 9 Schematic of the reference frame necessary to work across multiple Raspberry Pi cameras with a moving object

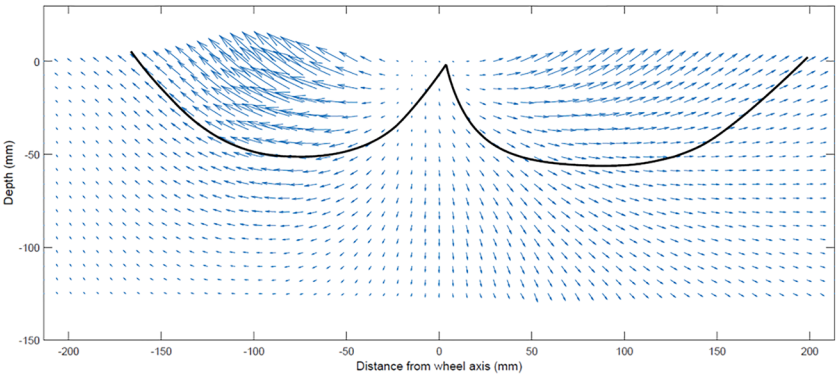

FIGURE 10 Soil displacement vector plot of a single layered pavement, load = 3.59 kN, achieved using Raspberry Pis

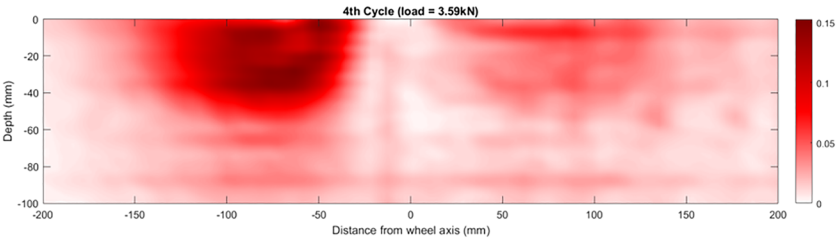

FIGURE 11 Shear strain of a single-layered pavement, load = 3.59 kN, achieved using Raspberry Pis

From this, the overall deformation mechanism was observed, which is shown for a single-layered pavement in Figure 10. This vectorial displacement plot is composed of images from three of the six cameras. The flow zone in front of and behind the tyre can be estimated from this plot and is sketched onto the figure. Using this displacement field, the shear strain plots were computed (Figure 11), which show the planes of failures around the moving tyre.

5 | CLOSURE

Geotechnical engineering research relies heavily on PIV/DIC techniques to measure subpixel soil displacements, from which strain is computed. Traditional methods for aligning multiple cameras in experimental set-ups and referencing to a known coordinate system present operational challenges, and the cameras typically used (machine vision cameras) are very costly. The use of ChArUco binary fiducial markers paired with low-cost SBC and cameras has been shown to have the following benefits:

- ChAruUco binary fiducial marker calibration facilitates the elimination of centroiding markers and therefore increases the speed of set-up and post-test processing.
- Custom machined windows can be reused since markers are not permanently affixed.

- Low-cost Raspberry Pi SBCs offer a viable and economic alternative to computer vision cameras, especially when the cost of set-up is considered.
- Practical improvements that SBC cameras offer over consumer-grade compact cameras (previously widely used in geotechnical engineering research) include precise control of camera parameters such as exposure, ISO, shutter speed and frame rate, all via software.
- Multicamera set-ups can have minimal or no overlap.
- The d/p (or D_{50}/p for sands) ratio can be maximised since the cameras can be placed closer to the observation window.
- The Raspberry Pi SBCs are practical for use in geotechnical experiments at 1-g or high-gravity environments and have been tested up to 100 g.

The Raspberry Pi cameras allow for custom set-ups to be created at low cost compared to traditional consumer-grade compact cameras or machine vision cameras. The benefits, such as custom programming interfaces and small size of the technology, allow for significantly increased scope for low-cost experimental set-ups to be created that still yield high-quality PIV/DIC data. The cost of entry for this system is approximately $125 USD per camera used and one-time costs of $175 for system peripherals. When arrays of these cameras are constructed to cover large experiment observation windows, the cost is an order of magnitude or more less than traditional PIV/DIC set-ups typically used for geotechnical engineering research yet offers comparable or better quality of PIV/DIC measurements owing to the ability to place these cameras closer to the target being measured.

ACKNOWLEDGEMENTS

The accelerated pavement and centrifuge tests were carried out with the invaluable assistance and experience of the technicians of the Schofield Centre at the University of Cambridge. The first author gratefully acknowledges the financial support of the National Science and Engineering Research Council of Canada (NSERC), Funding Reference Number PGSD3-517014-2018. The financial support of the Canadian Centennial Scholarship Foundation is also gratefully acknowledged.

ORCID

G. N. Eichhorn https://orcid.org/0000-0002-4764-8440
A. Bowman https://orcid.org/0000-0001-6457-647X
S. K. Haigh https://orcid.org/0000-0003-3782-0099
S. Stanier https://orcid.org/0000-0001-5671-2902

REFERENCES

[1] J. Orteu, *Opt. Lasers Eng.* **2009**, *47*(3-4), 282.
[2] G. Viggiani, S. A. Hall, *Adv. Exper. Techniq. Geomech.* Citeseer; **2004**:3.
[3] A. N. Schofield, *Géotechnique* **1980**, *30*(3), 227.
[4] Z. Chen, K. Li, M. Omidvar, M. Iskander, *Int. J. Phys. Modell. Geotech.* **2016**, *17*(1), 3.
[5] D. J. White, W. A. Take, M. D. Bolton, *Géotechnique* **2003**, *53*(7), 619.
[6] D. White, M. Bolton, *Géotechnique* **2004**, *54*(6), 375.
[7] W. A. Take, *Canadian Geotech. J.* **2015**, *52*(9), 1199.
[8] Y. Teng, S. A. Stanier, S. M. Gourvenec, *Int. J. Phys. Modell. Geotechn.* **2017**, *17*(1), 53.
[9] S. A. Stanier, D. J. White, *Geotech. Test. J.* **2013**, *36*(6), 1.
[10] S. Stanier, J. Dijkstra, D. Leśniewska, J. Hambleton, D. White, D. M. Wood, *Comput. Geotechn.* **2016**, *72*, 100.
[11] D. White, M. Randolph, B. Thompson, *Int. J. Phys. Modell. Geotech.* **2005**, *5*(3), 1.
[12] A. J. Bowman, S. K. Haigh, *Géotechnique* **2019**, *69*(7), 627.
[13] K. Q. Tan, Q. Y. Tung, F. H. Lee, S. H. Goh, *Japan. Geotech. Soc. Spec. Publ.* **2016**, *2*(74), 2553.
[14] I. Peerun, *Jap. Geotech. Soc. Spec. Publ.* **2016**, *2*(8), 354.
[15] P Kokkali, T. Abdoun, M Zeghal, *Soil Dyn. Earthq. Eng.* **2018**, *113*, 629.
[16] C. Heron, S. Haigh, G. Madabhushi, *in Seismic Evaluation and Rehabilitation of Structures*, Springer, Cham, Switzerland **2014**, 407.
[17] D. C. Brown, *Close-range Camera Calibration*, *37*, American Society of Photogrammetry and Remote Sensing **1976**.
[18] W. A. Take. **2004**, Ph.D. Thesis, University of Cambridge.
[19] S. Garrido-Jurado, R. Muñoz-Salinas, F. J. Madrid-Cuevas, M. J. Marín-Jiménez, *Pattern Recog.* **2014**, *47*(6), 2280.
[20] K. Pulli, A. Baksheev, K. Kornyakov, V. Eruhimov, *Queue* **2012**, *10*(4), 61.
[21] S. A. Stanier, J. Blaber, W. A. Take, D. J. White, *Can. Geotech. J.* **2016**, *53*(5), 727.
[22] M. Pagnutti, R. E. Ryan, G. Cazenavette, M. Gold, R. Harlan, E. Leggett, J. Pagnutti, *J. Electron. Imag.* **2017**, *26*(1), 013014.

[23] D. Jones, Picamera 1.13 documentation, https://picamera.readthedocs.io/en/latest/fov.html$\backslash$#hardware-limits, **2018**.
[24] E. M. C. Jones, M. A. Iadicola, A good practices guide for digital image correlation, International Digital Image Correlation Society **2018** https://doi.org/10.32720/idics/gpg.ed1
[25] J. Garnier, C. Gaudin, S. M. Springman, P. J. Culligan, D. Goodings, D. Konig, B. Kutter, R. Phillips, M. F. Randolph, L. Thorel, *Int. J. Phys. Modell. Geotech.* **2007**, *7*(3), 1.
[26] G. N. Eichhorn, S. K. Haigh, in Proceedings of the 9th International Conference on Physical Modelling in Geotechnics (ICPMG), Balkema, London **2018**.

How to cite this article: Eichhorn GN, Bowman A, Haigh SK, Stanier S. Low-cost digital image correlation and strain measurement for geotechnical applications. *Strain*. 2020;e12348. https://doi.org/10.1111/str.12348

APPENDIX A: SET-UP COSTS

The equipment required to construct a system similar to the ones described in this document is listed in Tables A1 and A2. There are additional considerations for materials required to connect and mount the cameras on a frame for use in either 1-*g* or a centrifuge environment; these have not been included in this accounting.

TABLE A1 Equipment required per camera

Item description	Item number	Supplier	Unit cost
Ultrathin HDMI cable	AV23487	OneCall	£6.40
Raspberry Pi 3 Model B+	1373331	RS Components	£24.98
MicroSD card	1239689	RS Components	£16.16
Raspberry Pi Camera Model 2.1	9132664	RS Components	£21.49
Ethernet cable	557-262	RS Components	£2.34
FFC to HDMI boards		Tindie	£11.00
2-pin socket power connector	4260953	RS Components	£3.86
2-pin plug power connector	4261114	RS Components	£4.34
2-pin cable connector for triggering wire	7345423	RS Components	£5.57
2-pin box mount socket for triggering wire	7345436P	RS Components	£4.82
40-way IDC connector for triggering wire	1103924	OneCall	£0.82
		Total cost	£101.78

TABLE A2 One-off items

Item description	Item number	Supplier	Unit cost
Crimp pins 10 per bag (does 5 Pis)	4261316	RS Components	£7.15
Crimp sockets 10 per bag (does 5 Pis)	4261293	RS Components	£5.18
Triggering junction box (good for 12 connectors)	4571231	RS Components	£14.56
Solid-state relay	2912466	RS Components	£15.76
Ethernet hub	1218128	RS Components	£42.97
Bag of 50 M3 hex pillars	325716	RS Components	£14.50
Spiral wrap for triggering wire	305510	RS Components	£16.12
4-way amphenol socket (master trigger wire)	872-1594	RS Components	£19.12
4-way amphenol plug (master trigger wire)	872-1446	RS Components	£7.84
		Total cost	£143.20